IEEE/CSC & ESAS European Superconductivity News Forum (ESNF), No. 15, January 2011
The published version of this manuscript appeared in *IEEE Transactions on Applied Superconductivity* **21**, Issue 3, 1926 - 1929 (2011)

Simulation of Interstrand Coupling Loss in Cable-In-Conduit Conductors With JackPot-AC

E. P. A. van Lanen and A. Nijhuis

***Abstract*—Within the framework of the design analysis of ITER PF coil joints, a model is developed that simulates the coupling loss between strands in a cable-in-conduit conductor (CICC). The present version of this model can simulate these losses in a cable section, subjected to any type of time-changing background field. It calculates the trajectories of all strands in the CICC, and uses this as the foundation for the electrical properties of the model, including strand transport properties, saturation and shielding. The simulation results are first compared with measurements on sub-size CICCs with different strand coating, which affects the interstrand resistance. In all but one of these simulations, the coupling loss time constants are lower than the measured values. A better agreement is obtained with the simulation of an ITER PF1 conductor, subjected to Twente Press experiments. For this simulation, only one final stage sub-cable is used, assuming that coupling currents between them is negligible due to the stainless steel wraps around them.**

***Index Terms*—CICC, coupling loss model, ITER, superconducting strands.**

I. Introduction

THE ITER tokamak contains six Poloidal Field (PF) coils to provide shaping and vertical stability of the plasma. They are designed with NbTi Cable-In-Conduit Conductors (CICCs), which are wound in double-pancakes, and connected in series with joints at the outer diameter [1]. Although stability analysis of these coils concluded that they will operate successfully within the specified temperature margin [2], [3], a more detailed analysis on the coil joints was also recommended [4]. There are essentially two reasons for this: First, the transport current is not fully transposed in the cable inside the joint, and close to it, making this region more vulnerable for instability [5], [6]. The second reason concerns the orientation of the background field with respect to the joints. The joints are placed in a position where they are expected to suffer the least from the longitudinal component of the PF coil's field. However, the loss due to other components of the background field, not only from the same PF coil, but also from other coils in the system, has not yet been investigated.

Estimating the effect from the current non-uniformity and the field orientation on the thermal stability of the joints requires a highly detailed model. Such a model was already developed earlier to analyze the DC behavior of CICCs [7]. This model (JackPot) accurately calculates the trajectories of all strands, and deduces all electrical properties from this. It is fully based on experimentally determinable conductor properties, such as strand parametric scaling laws and interstrand contact resistances. It has been used successfully to explain the differences between short and long length samples of ITER PF conductors [8], and is now being expanded with time-dependent components.

This paper describes the first step, in which only a short length of CICC is considered, which is not connected to a power source, and placed in a homogeneous background field that changes in time. This makes it already possible to simulate coupling loss measurements on cable sections in a solenoid or dipole magnet, and to perform parametric studies.

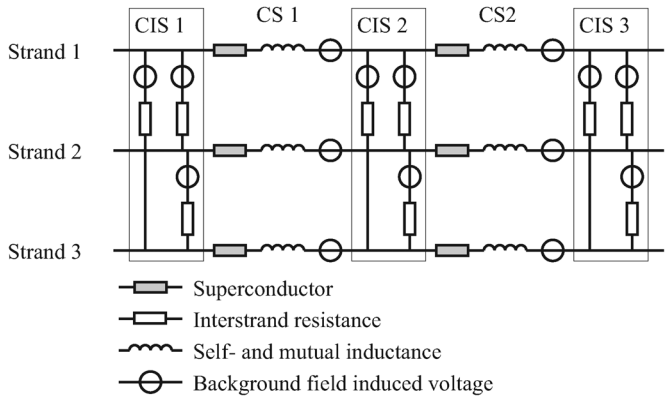

Fig. 1. Illustration of the CICC division in Cable Sections (CS), separated by Cable Intersections (CIS).

II. Model Description

Similar to other models [6], [9], [10], JackPot-AC simulates the CICC as a network of (mutual) inductances, induction voltage sources and two types of resistors; one that represents the electrical contacts between strands, and one that involves the superconducting strand properties (see Fig. 1). The backbone of the model is the cabling subroutine. It calculates the coordinates of the central axes of the strands, which are used to determine many of the electrical properties [7]. For example, an interstrand conductance is only present between strands if they are close enough together.

The strand trajectories are now also used to calculate the mutual inductances. For this, it is assumed that the coupling takes place between all piecewise linear sections that represent the strands, including the sections that belong to the same strand. The calculation of a section's self inductance is done with the theory described in [11]. The total self-inductance of a single

Manuscript received August 03, 2010; accepted September 25, 2010. This work was supported by ITER under Service Contract No. UT-ITER/CT/09/4300000070.

The authors are with the Faculty of Science and Technology, University of Twente, 7500 AE Enschede, the Netherlands (e-mail: e.p.a.vanlanen@tnw.utwente.nl).

Digital Object Identifier 10.1109/TASC.2010.2082474

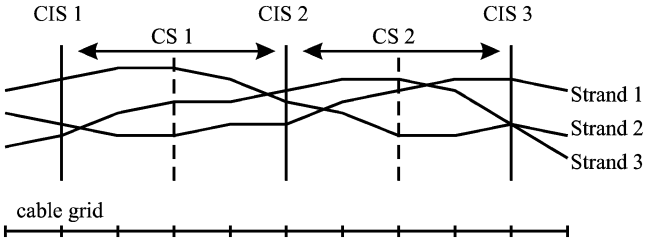

Fig. 2. Different grids used by JackPot-AC. The electrical properties of the cable (e.g. interstrand resistances and mutual conductances) are calculated using the fine cable grid; voltages and currents are calculated at the Cable Intersections (CIS) and Cable Sections (CS), respectively.

strand is thus the sum of self-inductances of its sections, plus the mutual inductances between them.

Since the strand sections are considered as one dimensional objects, the general equation for calculating the mutual inductance M_{ij} between strand sections i and j—which involves a double volume integral—can be simplified to the double line integral

$$M_{ij} = \frac{\mu_0}{4\pi} \int_{S_j} \int_{S_i} \frac{\mathbf{u}_i \cdot \mathbf{u}_j}{|\mathbf{r}_{ij}|} dl_i dl_j, \tag{1}$$

where S_i and S_j in are the lengths of strand sections i and j, respectively, $\mathbf{u}_i$ and $\mathbf{u}_j$ are their tangential vectors and $\mathbf{r}_{ij}$ is the distance between them. Equation (1) is re-written as

$$\mathbf{M}_{ij} = \int_{S_j} \mathbf{u}_j \cdot \mathbf{K}_{ij} dl_j, \tag{2}$$

with

$$\mathbf{K}_{ij} = \frac{\mu_0}{4\pi} \int_{S_i} \frac{\mathbf{u}_i}{|\mathbf{r}_{ij}|} dl_i. \tag{3}$$

Equation (3) is solved analytically, whereas for Equation (2), the adaptive quadrature function quad from Matlab is used, with a tolerance of $1.0 \cdot 10^{-6}$. It has been verified with volume integrals of cylinders that the filament approach used in (1) is accurate also for strands that are in close proximity with each other, as long as their lengths are short.

The calculation of the induced voltages due to an external time-changing background field B_{ext} is done in a similar way as the mutual inductances between strands. In each branch p that can carry current, the induced voltage is calculated as

$$V_{ext,p} = \int_{S_p} \mathbf{u}_p \cdot \partial_t \mathbf{A}_{p,ext} dl_p, \tag{4}$$

where $\partial_t \mathbf{A}_{p,ext}$ is the time derivative of the magnetic vector potential of the background field on branch p, and S_p is the length of the current path.

Although the accuracy of the electrical properties benefit from short strand sections, the system size would easily become too large to solve. Instead, the cable is divided into larger sections along its axis, and voltages are only calculated on the section ends (cable intersections), and strand currents are constant inside sections (see Fig. 2).

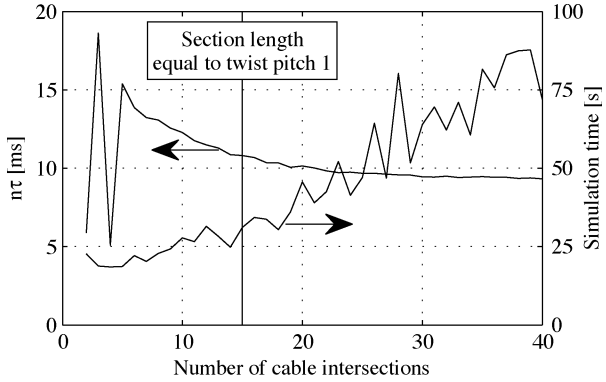

Fig. 3. Simulated coupling loss time constant and simulation time as function of the number of sections in which the 43.5 cm long cable is divided.

TABLE I
TYPES OF COATING USED FOR THE DIFFERENT SAMPLES, AND THE RESULTING GEOMETRIC MEAN INTERSTRAND RESISTANCES

Sample No.	Type	R [nΩ]
10	CuNi	100
13	Bare copper	20
14	Ni	154
15	Oxidised stabrite	174
16	Cr	2181

One of the many verifications of the model concerned the analysis of the effect of the number of cable intersections on the accuracy of the result. For this analysis, the coupling loss time constant nτ [12], [13], of a 43.5 cm long sub-size CICC, containing 36 strands and cabled in three stages, was calculated with different number of cable intersections. More details about this simulation are given in Section III. Fig. 3 shows the results, where the cable is characterized by nτ. As expected, nτ converges to a constant value as the number of cable intersections increases. However, as the system size increases, the computation time grows as well. In this example, a good trade-off between accuracy and computation time is found for cable intersections with a length that corresponds to about one half of the cable's shortest twist pitch, i.e. 30 cable intersections.

III. SIMULATION OF SUBSIZE NbTi CICCS

The model is verified with experiments carried out on five sub-size CICCs [14]. They are 43.5 cm long, and cabled in three stages of $3\times3\times4$ superconducting strands, with a specified twist pitch sequence of $29\times79\times141$ mm. The only design difference between the conductors is the coating on the strands, which results in different interstrand contact resistances, see Table I. Although the actual measurements were used to analyse the evolution of interstrand resistance and coupling loss during bending cycles, the analysis here focuses only on the initial state.

Each conductor was subjected to resistance measurements between 27 different sets of strands from different cabling stages. This experiment is first simulated, to fit the interstrand contact resistivity parameter ρ_{ss} [7] for each conductor. For this purpose, an optimization routine was used, that adjusts ρ_{ss} until the absolute difference between the measured and simulated set of interstrand resistances reaches a minimum. A good fit could

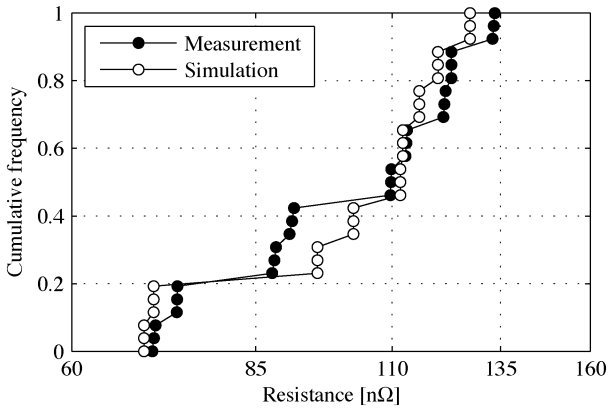

Fig. 4. Cumulative frequency distribution of measured and simulated interstrand resistances in Sample #10 [14].

TABLE II
MEASURED AND SIMULATED COUPLING LOSS TIME CONSTANTS IN MS

Sample No.	Measurement	Simulation
10	19.0	10.0
13	45.8	50.3
14	20.3	6.5
15	17.8	5.8
16	2.3	0.5

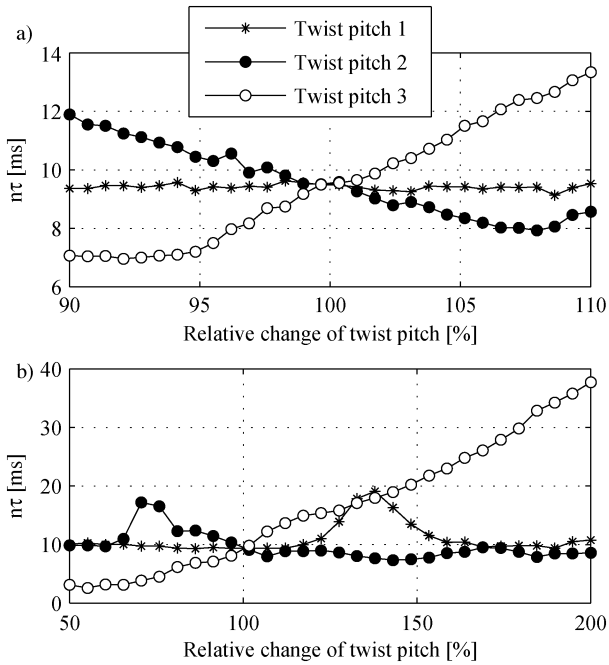

Fig. 5. (a) Effect of varying the twist pitch of one cabling stage on the coupling loss time constant of Sample #10. (b) The same as (a), but with a larger variation.

be found for all conductors (see Fig. 4), which indicates that the model gives an accurate description of the conductor.

Next, the conductors are subjected to a background field that changes sinusoidally in time. The field has an amplitude of 0.4 T, and its frequency ranges from 0.02 to 0.08 Hz. Since the model does not yet take hysteresis and inter-filament losses of strands into account, these components were subtracted from the measured power dissipation per unit volume, to make a comparison between the measured and simulated interstrand coupling loss possible. Table II summarizes the results, and it appears that only the simulation result for Sample #13 matches well with the measurement, whereas all other simulated coupling loss time constants are two to almost five times lower.

Variation in the twist pitches can be an explanation for the differences between measured and simulated coupling losses. Although the interstrand resistances for the simulations are matched to those in the measurements, the actual twist pitches of the different cabling stages have not been measured yet. To investigate what happens if the twist pitch of a cable is different, we carried out a series of simulations of Sample #10, each with a change in only one of the sub-cable twist pitches. Since we assume that the ρ_{ss} values derived from the interstrand resistance simulations are characteristic for the type of strand coatings, this value was the same in all simulation. Fig. 5(a) shows that a small, but realistic variation in the twist pitch of one cabling stage can double the $n\tau$ value, which might bring them closer to the measured values [14]. Therefore, the actual twist pitches of the tested cables will be measured for further verification.

Fig. 5(a) also shows that changing the twist pitch of the first cabling stage has negligible effect on $n\tau$, and that increasing the final stage twist pitch leads to an increase of $n\tau$. This is in agreement with the generally accepted rule that larger pitches lead to higher losses. However, the figure also shows that increasing only the twist pitch of the second cabling stage leads to a decrease in $n\tau$. When changing the twist pitch over a wider range [see Fig. 5(b)], it appears that this counter-intuitive observation is the result of interference effect of the multi-stage cable. This interference may also be affected by the length of the cable, but this was not investigated yet. Once it can be confirmed that the length is such that it has no influence on the results, the model opens opportunities for optimizing the cable pattern with respect to coupling losses.

IV. LOSS SIMULATION OF AN ITER PF CONDUCTOR

The following example shows the simulation result of a scenario that has been used with the PFCI, in which the background field of 4 T is dumped exponentially towards zero with a time constant of 5.68 s. The simulation considers only one petal (sub-cable from the final cabling stage) of the CICC design that is used for the PF1 and PF6 coils (see Fig. 6). For simplification, we assume that coupling currents between petals can be neglected due to the relatively high resistance of the stainless steel petal wraps. In addition, post processing of the simulation data revealed that the self-field of a petal is too low to have a shielding effect on its neighbor petals. Like in the previous examples, the simulated cable section ends are not connected to a power source. Its length is 400 mm, which is the same as a Twente Press sample [15], and the (constant) temperature is 4.2 K.

During cycling of the transverse load on the conductor, the interstrand resistance first rises to a maximum at about 100 cycles, after which it decreases to smaller values [15]. These values were used to derive ρ_{ss} for the simulations with the same procedure as described in Section III. It has a strong effect on the coupling loss time constant, as can be seen in Fig. 7. Although the

Fig. 6. Illustration of the coordinates of the 240 strands in the CICC used for the simulation of PF conductor.

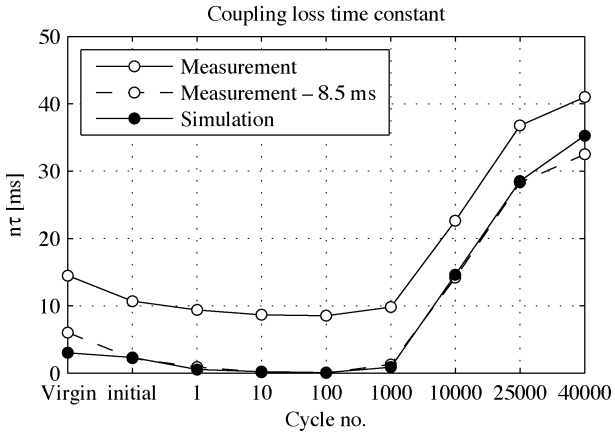

Fig. 7. Measured and simulated coupling loss time constant of an ITER PF1 conductor during cycling.

measured nτ reaches a minimum, it does not go to zero, because the interfilament coupling inside the strands is not affected by the loading. This loss component is not included in the model, thus the simulated nτ does approach zero at 100 cycles. When 8.5 ms is subtracted from the measured data, the simulation and measurement show an excellent agreement. This confirms that the nτ of the strands used in this cable is 8.5 ms.

V. Conclusion

With the present version of JackPot-AC, it is possible to carry out interstrand coupling loss simulations of short sections of CICCs, subjected to any time-changing background field. This comprises the computation of the local power dissipation by taking into account e.g. the strand transport properties, saturation and shielding. This is an important improvement compared to the phenomenological model with multiple time constants, each in fractions of the cable volume, as proposed earlier.

Simulation of five sub-size CICCs with different strand coatings resulted in a lower coupling loss time constant than the measured values, for all but one cable. Search for an explanation for this discrepancy is ongoing. If the twist pitches of the sub-cable stages are actually different than the values given by the manufacturer, they would have to be larger than 10% to account for the discrepancy. A better result is obtained with the simulation of Twente Press measurements on an ITER PF1 conductor. This simulation was done on only one of its final stage sub-cables, using the assumption that the coupling currents between them are negligible, due to the stainless steel wraps around them. In this simulation, the evolution of the measured coupling loss time constant during cycling coincides well with the simulated one.

References

[1] N. Mitchell *et al.*, "The ITER Magnet System," *IEEE Trans. Appl. Supercond.*, vol. 18, pp. 435–440, 2008.

[2] Y. Ilyin, D. Bessette, E. Zapretilina, C. Luongo, F. Simon, B. Su Lim, and N. Mitchell, "Performance analysis of the ITER poloidal field coil conductors," *IEEE Trans. Appl. Supercond.*, vol. 20, pp. 415–419, 2010.

[3] D. Bessette, L. Bottura, A. Devred, N. Mitchell, K. Okuno, and Y. Nunoya, "Test results from the PF conductor insert coil and implications for the ITER PF system," *IEEE Trans. Appl. Supercond.*, vol. 19, pp. 1525–1531, 2009.

[4] D. Ciazynski and A. Martinez, "Electrical and thermal designs and analyses of joints for the ITER PF coils," *IEEE Trans. Appl. Supercond.*, vol. 12, pp. 538–542, 2002.

[5] P. Bruzzone, M. Bagnasco, D. Bessette, D. Ciazynski, A. Formisano, P. Gilson, F. H. Hurd, and Y. Ilyin, "Test results of the ITER PF insert conductor short sample in SULTAN," *IEEE Trans. Appl. Supercond.*, vol. 15, pp. 1351–1354, June 2005.

[6] Y. Ilyin, A. Nijhuis, and H. H. J. ten Kate, "Interpretation of conduit voltage measurement on the poloidal field insert sample using the CUDI-CICC numerical code," *Cryogenics*, vol. 46, pp. 517–529, 2006.

[7] E. P. A. van Lanen and A. Nijhuis, "JackPot: A novel model to study the influence of current non-uniformity and cabling patterns in cable-in-conduit conductors," *Cryogenics*, pp. 139–148, 2009.

[8] E. P. A. van Lanen and A. Nijhuis, "Simulation of the ITER poloidal field coil insert DC performance with a new model," *Fusion Eng. Des.*, pp. 1912–1915, 2009.

[9] M. Ciotti, A. Nijhuis, P. L. Ribani, L. Savoldi Richard, and R. Zanino, "THELMA code electromagnetic model of ITER superconducting cables and application to the ENEA stability experiment," *Supercond. Sci. Technol.*, vol. 19, pp. 987–997, 2006.

[10] N. Mitchell, "Modelling of non-uniform current diffusion coupled with thermohydraulic effects in superconducting cables," *Cryogenics*, vol. 40, pp. 637–653, 2000.

[11] F. W. Grover, *Inductance Calculations*. New York: Dover publications, inc, 1946.

[12] M. N. Wilson, *Superconducting Magnets*. New York: Oxford University Press Inc., 1997.

[13] A. Nijhuis, N. H. W. Noordman, H. H. J. Ten Kate, N. Mitchell, and P. Bruzzone, "Electromagnetic and mechanical characterisation of ITER CS-MC conductors affected by transverse cyclic loading, Part 1: Coupling current loss," *IEEE Trans. Appl. Supercond.*, vol. 9, pp. 1069–1072, 1999.

[14] A. Nijhuis, H. H. J. Ten Kate, J. L. Duchateau, and P. Decool, "Control of contact resistance by strand surface coating in 36-strand NbTi CICCs," *Cryogenics*, vol. 41, pp. 1–7, 2001.

[15] Y. Ilyin *et al.*, "Effect of cyclic loading and conductor layout on contact resistance of full-size ITER PFCI conductors," *IEEE Trans. Appl. Supercond.*, vol. 15, pp. 1359–1362, June 2005.